Neurochemical Research (2020) 45:437–454
https://doi.org/10.1007/s11064-019-02935-w

ORIGINAL PAPER

Dendrobium Alkaloids Promote Neural Function After Cerebral Ischemia–Reperfusion Injury Through Inhibiting Pyroptosis Induced Neuronal Death in both In Vivo and In Vitro Models

Daohang Liu[1] · Zhi Dong[1] · Fei Xiang[1] · Hailin Liu[1] · Yuchun Wang[1] · Qian Wang[1] · Jiangyan Rao[1]

Received: 6 April 2019 / Revised: 10 December 2019 / Accepted: 15 December 2019 / Published online: 21 December 2019

Abstract

Pyroptosis is a newly identified lytic form of programmed cell death which is characterized by plasma membrane blebbing and rupture. Pyroptosis occurs in cerebral ischemia injury, and contributes to the activation and secretion of the inflammatory cytokines interleukin (IL)-1β, IL-18, and IL-6. Previous reports have found that Dendrobium alkaloids (DNLA) can exert neuroprotective effects against oxygen–glucose deprivation/reperfusion (OGD/R) damage in vitro, but the mechanisms underlying these effects remain elusive. In this study, we investigated whether DNLA exerted therapeutic benefits against cerebral ischemia–reperfusion (CIR) damage via ameliorating pyroptosis and inflammation. OGD/R damage was induced in HT22 cells pretreated with DNLA (0.03, 0.3, or 3 mg/ml, 24 h prior to OGD/R), MCC950 (10 ng/ml, 1 h prior), and VX765 (10 ng/ml, 1 h prior). Neuronal apoptosis, necrosis, pyroptosis, and pathological changes were analyzed 24 h following OGD/R. Further to this, male C57/BL mice pretreated with different concentrations of DNLA (0.5 or 5 mg/kg, ip.) for 24 h and VX765 (50 mg/kg, ip., 1 h before CIR) underwent transient middle cerebral artery occlusion and reperfusion. We found that DNLA pretreatment resulted in a lower neurologic deficit score, a reduced infarct volume, fewer pyroptotic cells, and reduced levels of inflammatory factors 24 h after CIR. Furthermore, DNLA administration also reduced the levels of the pyroptosis-associated proteins Caspase-1 and gasdermin-D, particularly in the hippocampal CA1 region. Similar decreases were observed in the levels of the inflammatory factors IL-1β, IL-6, and IL-18. OGD/R-associated ultrastructural damage was seen to improve following DNLA administration, likely due to the regulation of the tight junction protein Pannexin-1 by DNLA. Overall, these findings demonstrate that DNLA can protect against CIR damage through inhibiting pyroptosis-induced neuronal death, providing new therapeutic insights for CIR injury.

Keywords Dendrobium alkaloids · Pyroptosis · Inflammation · Ischemic–reperfusion injury · Caspase-1 · GSDMD

Introduction

Acute cerebral ischemic stroke is a severe neurological injury caused by thrombogenesis in the cerebral circulation which deprives the brain of nutrients and oxygen. This can lead to immobility, disability, and even death [1]. The only therapeutic option currently available for this disease is thrombolysis using recombinant tissue-plasminogen activator. This, however, has significant shortcomings, namely a narrow therapeutic time window of just

✉ Zhi Dong
100798@cqmu.edu.cn

Daohang Liu
dorian.lieu@gmail.com

Fei Xiang
731432953@qq.com

Hailin Liu
719204899@qq.com

Yuchun Wang
347417946@qq.com

Qian Wang
2419634277@qq.com

Jiangyan Rao
1107608504@qq.com

[1] Chongqing Key Laboratory of Biochemistry and Molecular Pharmacology, College of Pharmacy, Chongqing Medical University, District of Yuzhong, Chongqing 400016, China

4.5 h after the onset of symptoms and the potential risk of symptomatic intracranial hemorrhage [2]. Increasing evidence has suggested that inflammation plays a major role in ischemic stroke [3]. Presently, novel treatment strategies for acute ischemic stroke are urgently required.

Pyroptosis is a newly identified inflammatory form of programmed cell death. It is characterized by cell swelling and lysis, plasma membrane disruption, and the release of pro-inflammatory cytokines, ultimately inducing an inflammatory response after ischemic stroke [4]. It is well established that necrosis is a form of programmed cell death involved in stroke, and is mainly triggered by the mixed lineage kinase domain-like protein [5]. Pyroptosis is also known as caspase-1- or caspase-11-dependent programmed cell death, and is characterized by the formation of nonselective plasma membrane ion channels. A different type of ion channels are formed in necroptosis, which allow the influx of selected ions to induce cell swelling [6]. Pyroptosis can be triggered by the activation of various inflammasome complexes such as Nod-like receptor 3 (NLRP-3) [7] and the tight junction protein Pannexin-1 [8]. Previous studies have shown that high extracellular K^+ and mitochondrial reactive oxygen species (ROS) levels induced by arterial ischemic stroke can activate Caspase-1 via NLRP-3 eand Pannexin-1 [8–10]. Caspase-1 is an essential precursor of pyroptosis which cleaves and activates the pore-forming effector molecule gasdermin-D (GDSMD) [11, 12]. Cleavage of GDSMD separates its N-terminal product (GSDMD-NT) and C-terminal fragment (GSDMD-CT). GSDMD-NT then binds to the plasma membrane, generating large pores [13, 14]. These membrane pores then facilitate the release of cytoplasmic contents such as interleukin (IL)-1β, IL-6, and IL-18, which are inflammatory mediators of pyroptosis. Previous studies have focused on Caspase-1 as a promising target for alleviating cerebral ischemia–reperfusion (CIR)-induced brain inflammation. However, these studies failed to demonstrate the role of pyroptosis in CIR injury, and did not elucidate the balance between apoptosis, necrosis, and pyroptosis in murine stroke model [15, 16].

Belnacasan (VX765), a potent and selective inhibitor of Caspase-1, is converted into the active drug VRT-043198 in vivo, and can exert a strong anti-inflammatory action through inhibiting the release of IL-1β, IL-6, and IL-18 [17, 18]. VX765 has been shown to slow down the progression of neurodegeneration, Aβ accumulation, and neuroinflammation in a mouse model [19, 20]. Furthermore, the selective, small-molecule inhibitor MCC950 has been postulated to reduce infarction through blocking both canonical and non-canonical NLRP3 activation, thus down-regulating Caspase-1 and diminishing the inflammatory response [15, 21, 22]. Hence, the effects of both VX765 and MCC950 demonstrate that pyroptosis is associated with CIR injury, identifying a potential novel therapeutic strategy for brain ischemic diseases.

Dendrobium alkaloids (DNLA) have been reported to exert therapeutic effects against cataracts, retinal inflammation, and fungi-induced inflammation. DNLA are active components extracted from the famous traditional Chinese herbal medicine Dendrobium [23, 24]. The primary active ingredients of Dendrobium include alkaloids, stilbenoids, glycosides, and polysaccharides [25]. Significant research has been conducted into the anti-oxidative, anti-microbial, anti-Aβ injury, and anti-inflammatory activities of DNLA [26–28]. Furthermore, previous studies have demonstrated that DNLA exerts neuroprotective effects against (OGD/R)-induced injury in primary cultures of rat cortical neurons [29], though the mechanisms of action underlying these effects have not yet been elucidated.

This study investigated the effects of DNLA on pyroptotic cell death in vivo and in vitro, and evaluated the involvement of CIR-associated Caspase-1/GSDMD signaling. Ultimately, this study aimed to cast light on an innovative putative clinical application of DNLA and elucidate potential novel treatments for stroke.

Results

DNLA Inhibit the Pyroptosis of HT22 Cells After OGD/R

We conducted a number of cell death assays [3-(4,5-dimethylthiazol-2-yl)-2,5-diphenyltetrazolium bromide (MTT) and lactate dehydrogenase (LDH) release] to investigate the existence of pyroptosis in HT22 cells after OGD/R in vitro [30]. Cell mortality rate and LDH release rate were significantly higher in the OGD/R group than in any of the DNLA groups. A significantly reduced LDH release rate was noted in the H DNLA group (high dose dendrobine alkaloids group, 3 mg/ml) (Fig. 1a and b; $^{**}P < 0.01$). Importantly, PEG3000 could block the membrane pores initiated by pyroptotic proteins according to previous proposal that large size PEG could block the pyroptotic pores [31], which also meant that PEG3000 could be used to identify the occurrence of pyroptosis. In comparison to the cell group challenged with OGD/R, cells pretreated with DNLA (3 mg/ml) exhibited significantly lower mortality and LDH leakage rates (Fig. 1a and b; $^{**}P < 0.01$). Cell mortality rate and LDH leakage rate were almost unchanged when PEG3000 (1%) was added into F12 nutrient medium, suggesting that PEG3000 (1%) did not influence cell survival rate. Interestingly, the group (OGD/R + PEG3000(1%) → Media) in which PEG3000 (1%) was added during OGD exhibited significantly lower mortality and LDH leakage rates than the group (OGD/R + Media → PEG3000(1%)) in which

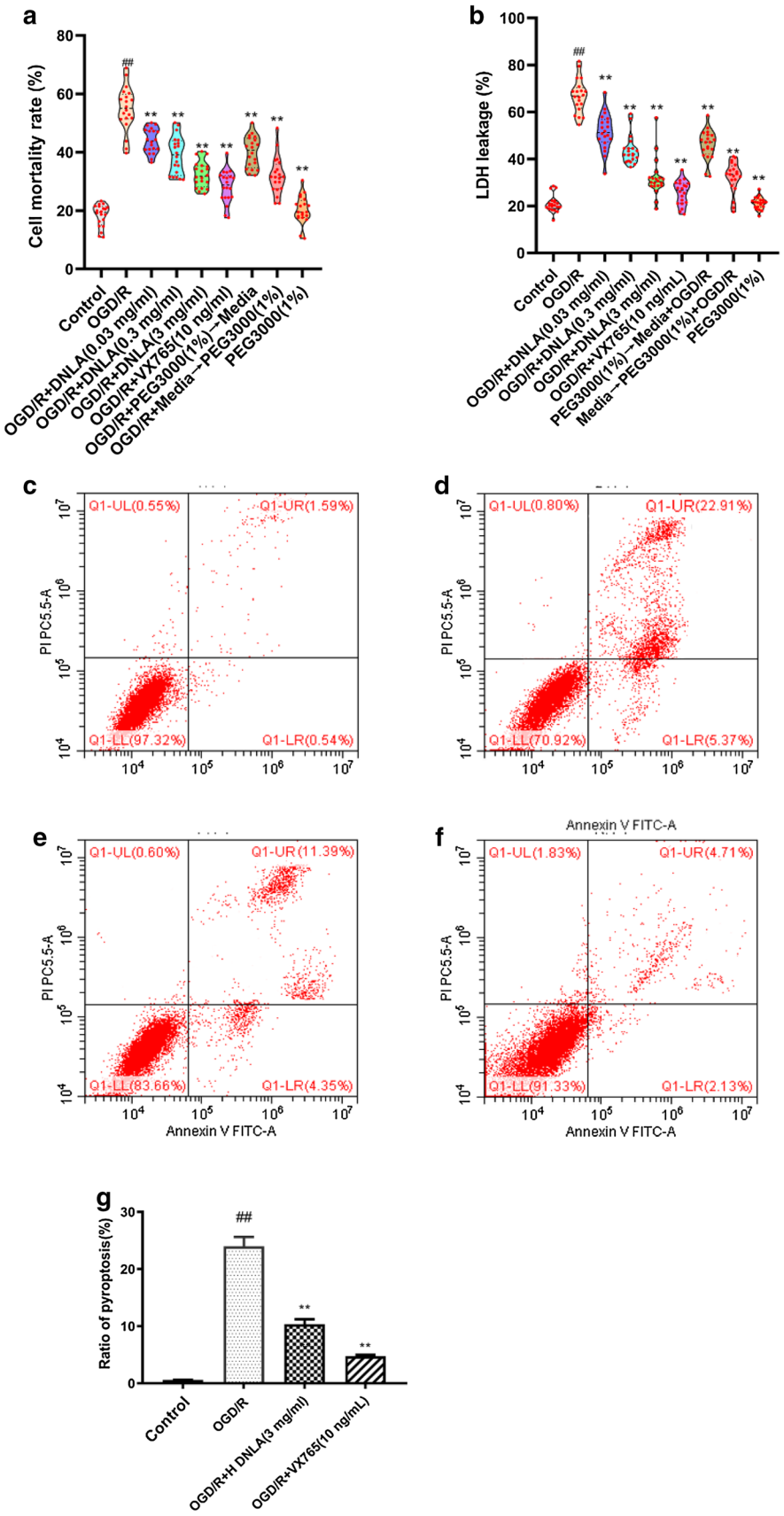

Fig. 1 Neuroprotective effect of DNLA on HT22 cells at 24 h after OGD/R (n = 20) in different groups. **a** Cell viability was evaluated by performing MTT staining. **b** LDH release analysis. **c**–**f** The quantity of necrotic cells and pyroptotic cells were analyzed by annexin V and PI staining. **c** Control group. **d** OGD/R group. **e** OGD/R+H DNLA group. **f** OGD/R+VX765 group $^{\#\#}P < 0.01$ versus control group; $^{**}P < 0.01$ versus OGD/R group. **g** Ratio of pyroptosis and necrosis. $^{\#\#}P < 0.01$ versus control group; $^{**}P < 0.01$ versus OGD/R group

PEG3000 (1%) was added into F12 nutrient medium after OGD/R (Fig. 1a and b; $^{**}P < 0.01$). Thus, pyroptosis progressed during the course of OGD. Similarly, VX765 (10 ng/ml), an inhibitor of Caspase-1, suppressed pyroptosis—the group of VX765-treated HT22 cells exhibited lower cell mortality and LDH release rates than the other groups (Fig. 1a and b; $^{**}P < 0.01$). In the VX765 group, cell mortality rate and LDH leakage rate decreased to 27.8% (±0.3%) and 27.4% (±0.7%), respectively. Collectively, our data implied that DNLA pretreatment improved neuronal function by inhibiting pyroptosis after OGD/R.

DNLA Relieve OGD/R-Induced HT22 Pyroptosis and Necrosis

In this experiment, pyroptotic cells exhibited PI and Annexin V double-staining (Fig. 1c–f; Q1-UR quadrant) [32]. In our results, the OGD/R group exhibited a higher pyroptosis rate than the control group. Both the H DNLA group (3 mg/ml) and the VX765 group exhibited significantly lower pyroptosis rates than the OGD/R group (Fig. 1c–f; $^{\#\#}P < 0.01$). Meanwhile, Annexin V positive staining and PI negative staining serves as a sensitive probe for flow cytometric analysis of cells that are undergoing apoptosis, but the apoptotic cells (Fig. 1c–f; Q1-LR) did not show significant differences, suggesting that DNLA played a vital neuroprotective role against OGD/R-induced pyroptosis.

DNLA Exert a Protective Effect Against OGD/R-Induced Pyroptotic Damage in HT22 Cells

To detect whether OGD/R-induced pyroptotic ultrastructural changes occurred in HT22 cells, we assessed cell membrane morphological features during different stages of OGD/R using scanning electron microscopy (SEM). In the OGD/R group, the cell membrane was severely destroyed, exhibiting asymmetric pyroptotic bodies and multiple foamy protrusions (Fig. 2a). Compared to the OGD/R group, HT22 cells in the control (DMSO) group exhibited less swelling and the pyroptosis-induced pores observed in the late stage of the OGD/R group were also visible (Fig. 2a). To further these SEM results, we stained for Caspase-1, the chief activator of pyroptosis. A greater number of Caspase-1-positive cells was noted in the OGD/R group than in the H DNLA (3 mg/

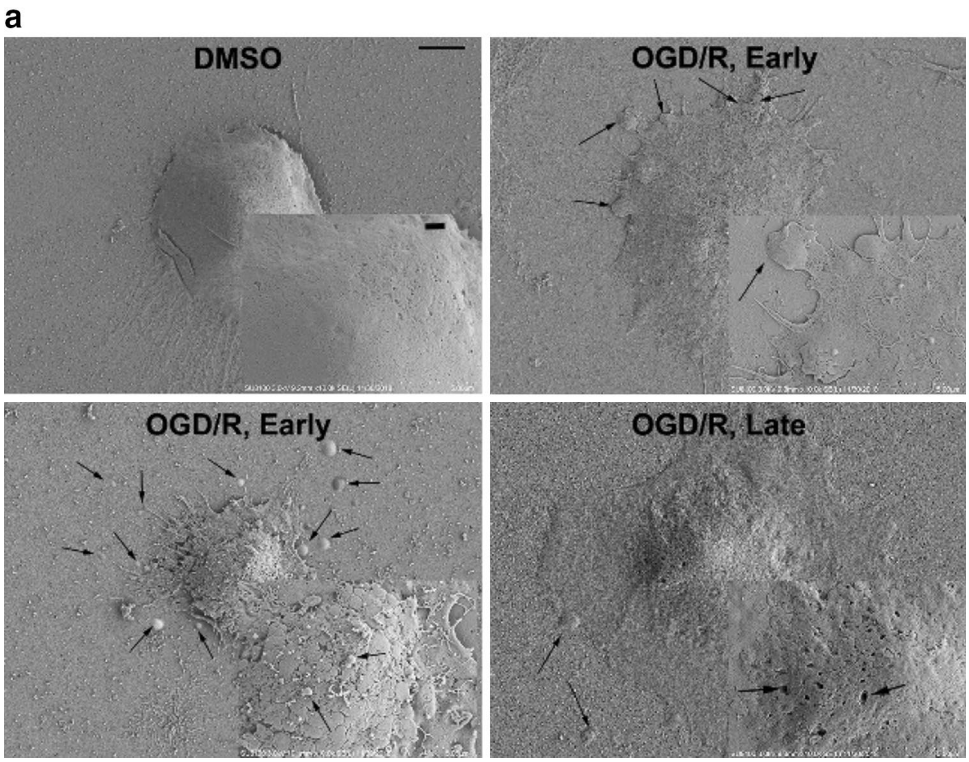

Fig. 2 Pyroptosis in HT22 cells initiated at the early stage of oxygen glucose deprivation/reperfusion (OGD/R) and cells were stained with double immunofluorescence labeling (green and blue) showed DNLA downregulates expression of Caspase-1 protein (green) in neurons. **a** Representative scanning electronic microscopy images of the morphological changes of HT22 cells treated as in OGD/R. Arrowheads point to the presence of foaming pyroptotic bodies released by HT22 cells in different stage. Scale bar, 5 μm. **b** Changes of pyroptotic protein Caspase-1 expression in HT22 cells during OGD. Detection of Caspase-1 in HT22 cells challenged with OGD/R by immunofluorescence assay (n = 5). Scale bar, 50 μm. **c** Quantification of green-labelled Caspase-1-positive cells. $^{\#\#}P < 0.01$ versus control group; $^{*}P < 0.01$ versus OGD/R group; $^{**}P < 0.01$ versus OGD/R group

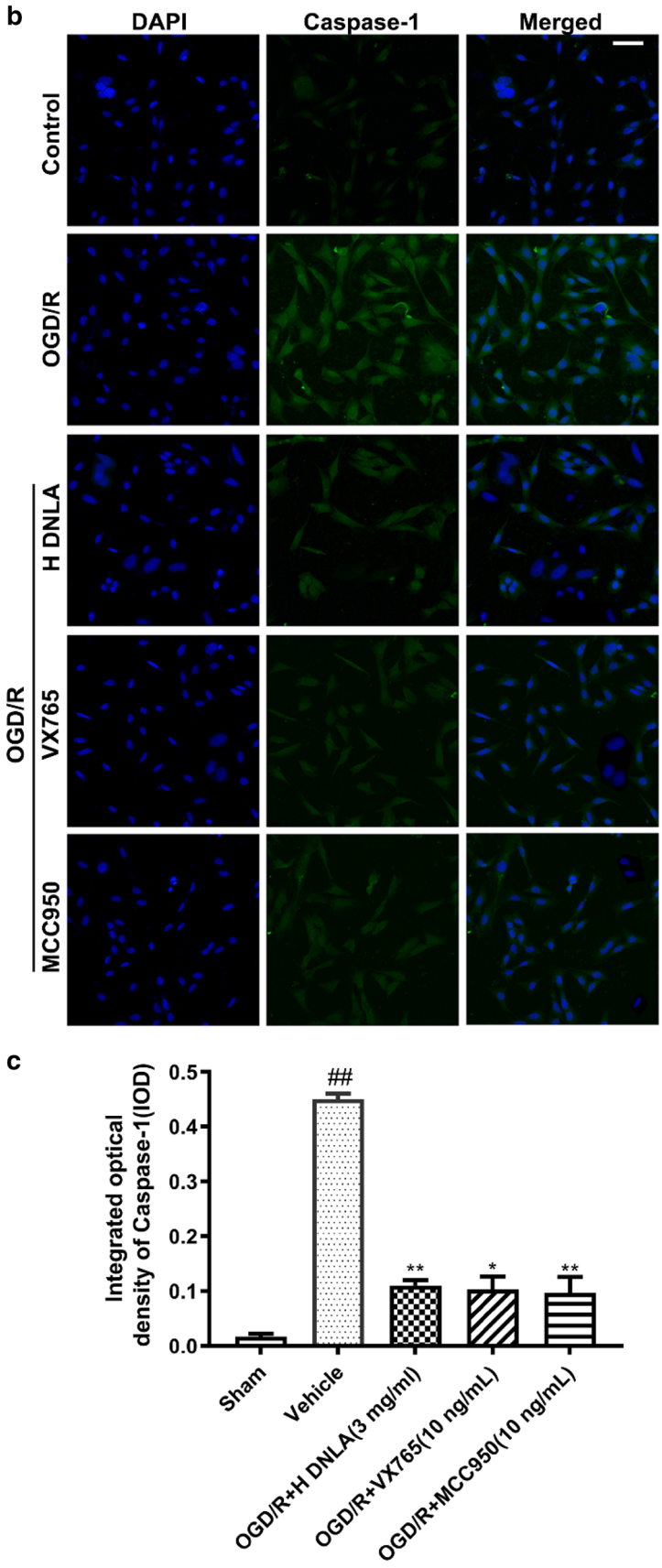

Fig. 2 (continued)

ml) group, VX765 group (10 ng/ml), and MCC950 group (10 ng/ml) (Fig. 2b). Taken together, these data suggest that OGD/R induced pyroptosis in HT22 cells, and DNLA exerted a beneficial effect against this OGD/R-induced pyroptotic damage.

DNLA Exert a Neuroprotective Effect Against CIR Injury in the MCAO Mouse Model

To investigate whether DNLA could ameliorate CIR injury, neurological deficit score and infarct volume were evaluated in the Sham group, CIR group, and DNLA groups (treated with 0.5 or 5 mg/kg DNLA). Compared to the CIR group, the L (0.5 mg/kg) and H (5 mg/kg) DNLA groups exhibited 8% and 15% smaller infarct volumes, respectively (Fig. 3a and b; $^{**}P < 0.01$). Meanwhile, the neurological deficit score of the CIR group was significantly higher than that of the Sham group. Compared to the CIR group, the neurological deficit scores of the L (0.5 mg/kg) and H (5 mg/kg) DNLA groups were significantly lower (Fig. 3c; $^{**}P < 0.01$). These results demonstrated that DNLA exerted a significant neuroprotective effect against neuronal CIR injury.

Magnetic resonance imaging (MRI) was used to detect the infarct volume in the mice brains. The MRI results agreed with the results of the TTC staining (Fig. 3c and d; $^{**}P < 0.01$). Taken together, these results demonstrated that DNLA improved neurological function in the mouse after CIR.

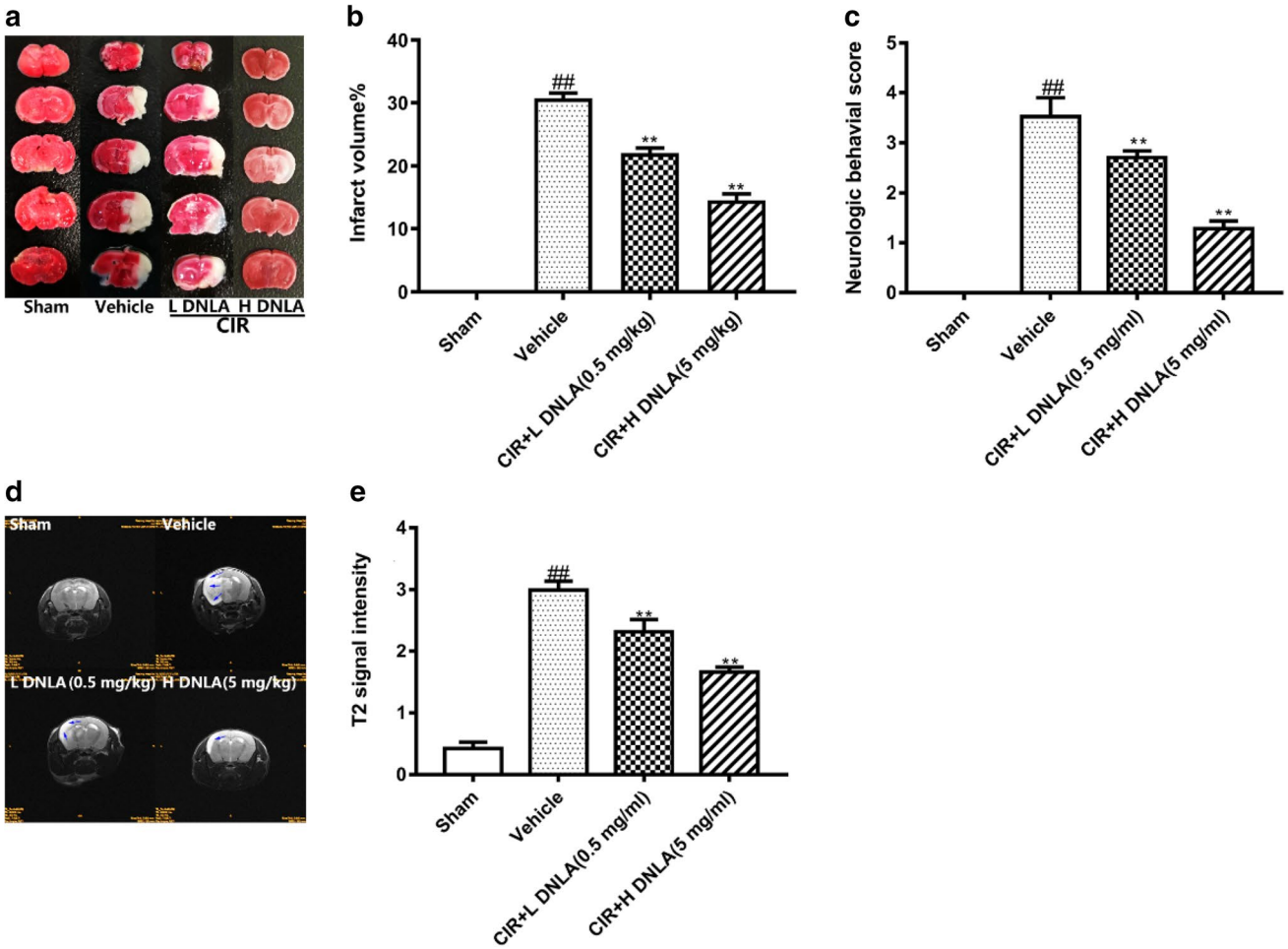

Fig. 3 Cerebral ischemic lesion volume and signal intensities were detected by 2,3,5-Triphenyltetrazoliumchloride (TTC) and T2-weighted magnetic resonance imaging (MRI) from the different groups; note that reductions in infarct volume and T2 signal intensity and alleviation of neurological deficits after cerebral ischemia–reperfusion were observed in C57/BL mice pretreated with DNLA (0.5 or 5 mg/ml). **a** Representative TTC stained brain sections showing areas of healthy tissue (red) and ischemic injury (white) of different group (n = 6). **b** Quantitative analysis of ischemic lesion volume. **c** Neurological severity scores of each group evaluated at 24 h after reperfusion. **d** Each image represents the MRI results of different groups—note the T2-weighted signal intensity evolution indicated by blue arrows. A larger and more intense white highlighted region represents more severe cerebral damage (n = 6). **e** T2 signal intensity were observed in different groups. $^{\#\#}P < 0.01$ versus Sham group; Sham = sham-operated group; vehicle = vehicle-operated CIR group; $^{**}P < 0.01$ versus Vehicle group

DNLA Mitigate a Component of CIR-Induced Pyroptotic Neuronal Death in the Mouse Cerebral CA1 Region

There are distinctive morphological differences between apoptosis, necroptosis, and pyroptosis. To investigate whether DNLA exerted a neuroprotective effect against CIR-induced cerebral injury, we employed Nissl staining to analyze changes in the diameter and number of neurons during CIR. Compared to the normal control mice, we noted an apparent decrease in neuronal density in the CA1 area (Fig. 4a and b) and an increase in neuronal diameter (Fig. 4a and c) after CIR. However, treatment with DNLA and VX765 limited the decrease in neuron number and maintained neuronal diameter within a normal range, retarding cell swelling (Fig. 4a–c). Thus, H&E stained slices were employed and analyzed using ultrahigh resolution fluorescent microscopy to further elucidate the forms of neuronal death occurring in the cerebrum after CIR. In the hippocampal CA1 region of the CIR group, we observed multiple small cerebral infarcts with apoptotic cells (membrane blebbing, shrunken soma, and concentrated nucleus), necrotic cells (intact nucleus, expanded soma like an over-inflated balloon), and pyroptotic cells (less swollen than necrotic cells, exhibiting a cabbage or fried-egg-like appearance with a detached nucleus in the center) (Fig. 4d). This was in sharp contrast to the Sham group, in which cells exhibited a normal appearance [6]. Notably, pyroptotic cells were densely distributed throughout the hippocampal CA1 region, but were rarely observed in the cortex (Fig. 4d). Furthermore, mice administered DNLA and VX765 exhibited pathological improvement and reduced cerebral damage after CIR (Fig. 4d). Together, these results indicated that pyroptotic brain cells coexisted with apoptotic and necrotic cells in the hippocampal CA1 region and parts of the cerebral cortex, and pyroptosis accounted for a certain proportion of neuronal death. Therefore, DNLA exerted an anti-pyroptotic effect in CIR-induced cerebral injury.

DNLA Inhibit the Pyroptosis-Associated Inflammatory Cascade by Regulating Proptosis-Related Protein Levels in Mice

Caspase-1 is responsible for the proteolytic maturation of IL-1β. VX765, an inhibitor of Caspase-1, was administered to C57BL mice to investigate whether pyroptosis-induced cerebral inflammation after CIR could occur in the absence of Caspase-1 and to determine the effect of DNLA on areas of brain damage. Compared to the Sham group, the expression of IL-1β, IL-6, and IL-18 was significantly increased in the MCAO mice 24 h after CIR (Fig. 5a and b; $^{\#}P < 0.05$, $^{\#\#}P < 0.01$). Compared to the CIR group, the DNLA groups and VX765 group all exhibited significantly lower IL-1β, IL-6, and IL-18 expression (Fig. 5a and b; $^{**}P < 0.01$, $^{*}P < 0.05$). These findings demonstrated that in mice, DNLA could ameliorate CIR-induced cerebral injury via the suppression of inflammation.

DNLA Exert a Neuroprotective Effect Against CIR Injury by Regulating the Pyroptotic Mastermind Caspase-1 In Vivo and In Vitro

Caspase-1 induces the release of a series of inflammatory cytokines and promotes GSDMD-dependent membrane pore formation, ultimately initiating pyroptosis. To identify whether Caspase-1 initiated neuronal pyroptosis after CIR and if DNLA exerted an anti-pyroptotic effect, the protein levels of Caspase-1, GSDMD, and GSDMD-C were measured in all five in vivo groups and six in vitro groups. Compared to the CIR vehicle group, the VX765 and H DNLA groups exhibited significantly lower Caspase-1 and GSDMD protein levels (Fig. 6a and c; $^{**}P < 0.01$, $^{*}P < 0.05$). In contrast, GSDMD-C expression was significantly increased in these groups (Fig. 6a and c; $^{*}P < 0.05$). As expected, the Western blot Caspase-1, GSDMD, and GSDMD-C results were consistent between the in vitro and in vivo experiments (Fig. 6b and d; $^{**}P < 0.01$, $^{*}P < 0.05$). Overall, DNLA preadministration substantially down-regulated the expression of Caspase-1 and retarded the pyroptosis of brain cells, attenuating CIR-induced cerebral damage. It could also be concluded that GSDMD cleavage by Caspase-1 was the executor of pyroptosis after CIR.

DNLA Ameliorate CIR In Vivo via Inhibiting Neuronal Pyroptosis

The levels of NLRP3, Caspase-1, and Pannexin-1 were detected by Western blot to further investigate the pyroptotic mechanism occurring in vivo. Compared to the Sham group, the CIR group exhibited significantly higher Caspase-1 and NLRP3 protein levels (Fig. 7a, b, and d; $^{\#}P < 0.05$, $^{\#\#}P < 0.01$). However, DNLA pretreatment significantly decreased Caspase-1 and NLRP-3 protein levels after CIR in vivo (Fig. 7a, b, and d; $^{**}P < 0.01$, $^{*}P < 0.05$). Strikingly, the Western blot results demonstrated reduced fluctuations in Pannexin-1 protein levels in the DNLA and MCC765 groups compared to the obvious decreases in Caspase-1 and NLRP-3 protein levels, likely due to enhanced protein glycosylation (Fig. 7a–d, $^{**}P < 0.01$, $^{*}P < 0.05$). These data indicate that Caspase-1 was down-regulated by DNLA, affecting cell morphogenesis and permeability. Thus, extracellular ATP liberation from Pannexin-1-related channels during pyroptosis in the mouse cerebral CA1 region was investigated using transmission electron microscopy (TEM) and immunofluorescence. When the hippocampal CA1 region was stained, the CIR group exhibited greater numbers of

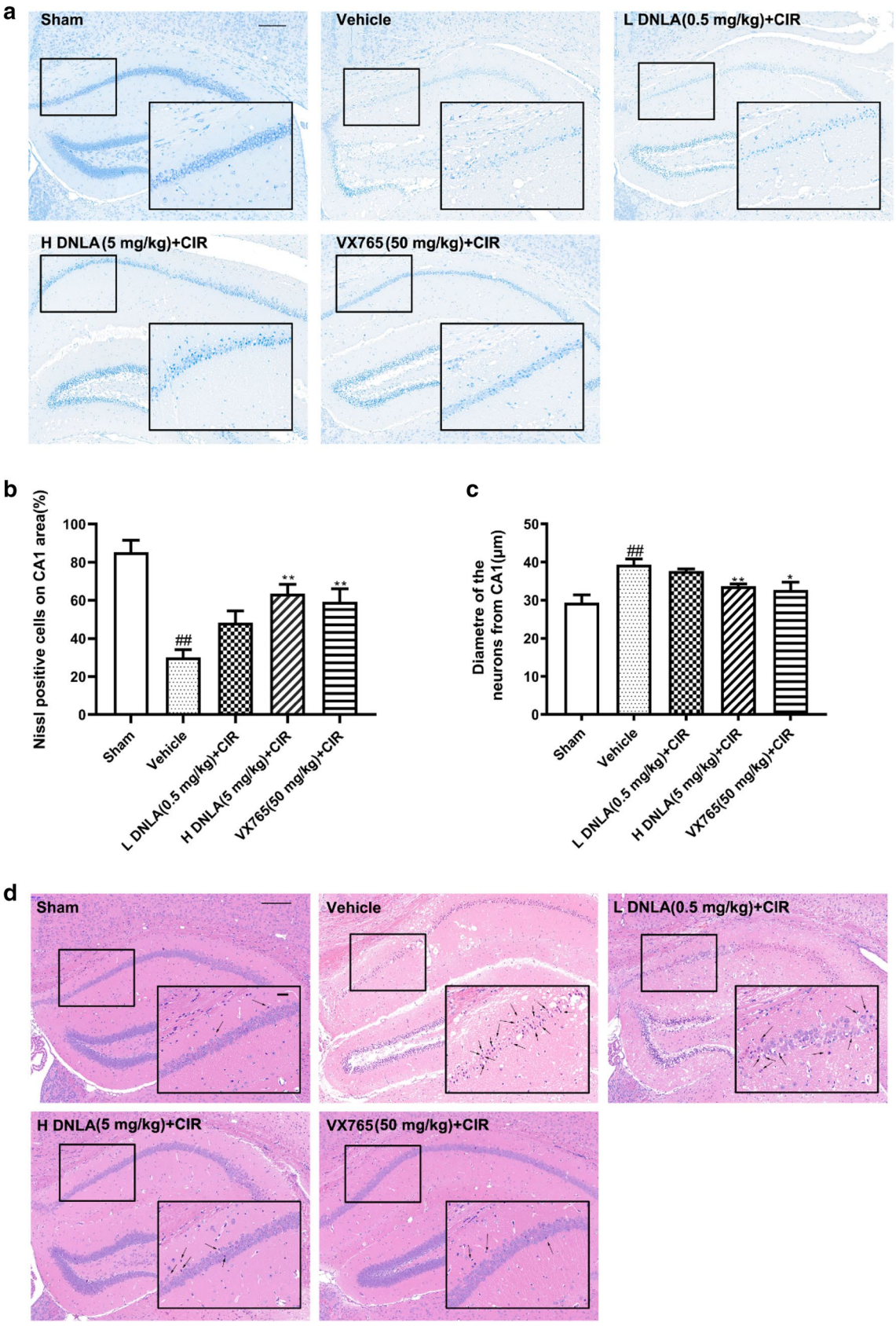
a
Sham
Vehicle
L DNLA(0.5 mg/kg)+CIR
H DNLA(5 mg/kg)+CIR
VX765(50 mg/kg)+CIR
b
Nissl positive cells on CA1 area(%)
100
80
60
40
20
0
##
**
**
Sham
Vehicle
L DNLA(0.5 mg/kg)+CIR
H DNLA(5 mg/kg)+CIR
VX765(50 mg/kg)+CIR
c
Diametre of the neurons from CA1(μm)
50
40
30
20
10
0
##
**
*
Sham
Vehicle
L DNLA(0.5 mg/kg)+CIR
H DNLA(5 mg/kg)+CIR
VX765(50 mg/kg)+CIR
d
Sham
Vehicle
L DNLA(0.5 mg/kg)+CIR
H DNLA(5 mg/kg)+CIR
VX765(50 mg/kg)+CIR

◂**Fig. 4** DNLA administration attenuate cerebral ischemia–reperfusion (CIR)-induced neuronal impairment in the hippocampal CA1 region in C57/BL mice. **a** Nissl-stained sections indicating that DNLA decrease CIR-induced neuronal death in the hippocampus of C57/BL mice (n = 3), scale bar, 100 μm. **b** Quantification of Nissl-positive neurons in each group. The number of Nissl bodies decreased notably after middle cerebral artery occlusion (MCAO) (n = 3), $^{\#\#}P < 0.01$ versus Sham group, $^{**}P < 0.01$ versus Vehicle group. **c** Analysis of the diameter of the neurons in the CA1 region among groups (n = 3), $^{\#\#}P < 0.01$ versus sham group, $^{**}P < 0.01$ versus Vehicle group, $^{*}P < 0.05$ versus Vehicle group. **d** Hematoxylin–eosin staining (H&E) staining of mouse brain slices and hippocampal CA1 region 24 h after MCAO was performed (n = 3), scale bar, 100 μm

red-stained Pannexin-1-positive cells and green-stained Caspase-1-positive cells than the H DNLA group, VX765 group, and MCC950 group (Fig. 8a and b). Compared to the Sham group, the CIR group also exhibited a greater number of swollen mitochondria and partly disintegrated and fractured myelin figures (Fig. 8c). DNLA treatment and VX765 treatment exerted protective effects on the mitochondria. These protective effects were also exerted by MCC950, the NLRP3-Caspase-1 pathway inhibitor (Fig. 8c). The data above demonstrated that DNLA could palliate CIR injury in vivo via inhibiting neuronal pyroptosis.

The Caspase-1 Inhibitor VX765 Desensitizes the Brain to CIR Injury

To further investigate the role DNLA play in cerebral protection after CIR, we muted Caspase-1 expression in mice by pre-administrating the Caspase-1 inhibitor VX765. The CIR+H DNLA+VX765 group exhibited a significantly decreased neurological deficit score, T2 signal intensity, and infarct volume compared to the CIR+H DNLA, CIR+VX765, and CIR groups (Fig. 9a–d; $^{\&}P < 0.05$, $^{\&\&}P < 0.01$). This also testified that acute CIR injury was conspicuously ameliorated in the CIR+H DNLA+VX765 group (Fig. 6a and c; $^{**}P < 0.01$, $^{*}P < 0.05$). Interestingly, the H DNLA and VX765 groups exhibited little difference with respect to T2 signal intensity, cerebral infarct volume, and neurobehavioral score, suggesting that DNLA and VX765 may act on the same target with the same function. Taken together, our data demonstrated that DNLA could protect against CIR injury in association with Caspase-1 inhibition.

Discussion

Pyroptosis, also known as Caspase-1-dependent programmed cell death, is a newly identified inflammatory form of programmed cell death that is triggered by microbial stimuli, calcium overload, and free radicals. Previous reports have demonstrated the neuroprotective effects of DNLA against OGD/R-induced impairment [28], though the mechanisms underlying these effects remain unclear. This study is the first to successfully demonstrate that pyroptosis occurs in CIR injury, and that DNLA can protect brain tissues from CIR damage via inhibiting pyroptotic cell death in vivo and in vitro. We demonstrated that DNLA can downregulate IL-1β, IL-6, and IL-18, diminishing the ischemic inflammatory cascade reaction, and can mute GSDMD and Pannexin-1 expression, delaying the lysis of neurons.

Cell death via different biochemical pathways produces distinct morphological and functional outcomes. The most studied and widely recognized forms of programmed cell death are apoptosis and necrosis [28, 33]. It is generally accepted that apoptosis is not associated with an inflammatory response, but is characterized by cell shrinkage, membrane blebbing, nuclear condensation, and the generation of apoptotic bodies. Necrosis is characterized by the formation of selective pores, membrane permeabilization, and plasma explosion [34, 35]. Pyroptosis has gained attention in the last few years, and is characterized by cytoplasmic flattening, mitochondrial and organelle swelling, the formation of non-selective pores, and the generation of pyroptotic bodies which are a similar size to apoptotic bodies. Although there is a clear difference in the morphologic features of apoptosis, necrosis, and pyroptosis, a number of different methods have been used to testify the existence of pyroptosis in ischemic vascular disease. Currently, immunofluorescence staining and flow cytometry are utilized to identify pyroptotic cells, and have been used to determine the forms of cell death that occur in the hippocampal CA1 region [36]. Surprisingly, the OGD/R group exhibited a slightly reduced apoptotic neuron death toll, demonstrating the suppression of apoptosis by pyroptosis, likely due to competition among apoptosis, pyroptosis, and necroptosis [37]. It has also been found that pyroptotic and necroptotic cells have distinct morphological features [6, 38]. Furthermore, LDH release, H&E staining, SEM, and TEM can be jointly conducted to give a morphological depiction of pyroptotic neuronal death [31, 39] in in vitro and in vivo experiments. In our study, the flow cytometry analysis demonstrated that pyroptosis, necrosis, and apoptosis are all involved in hypoxic-ischemic brain damage. Immunofluorescence and H&E staining demonstrated that in the hippocampal CA1 region, there are more pyroptotic neurons than apoptotic and necroptotic neurons, and this is reversed in the cerebral cortex. In addition, our research demonstrated a number of cellular ultrastructure changes of pyroptotic neurons, namely swollen mitochondria, the release of pyroptotic bodies, cabbage-like pyroptotic cell corpses, the formation of membrane pores, and less cell swelling than necrotic cells. In previous studies, it has been shown that PEG3000 endows cells with an anti-pyroptotic ability and can be used to distinguish pyroptosis from necrosis via blocking non-selective membrane pores.

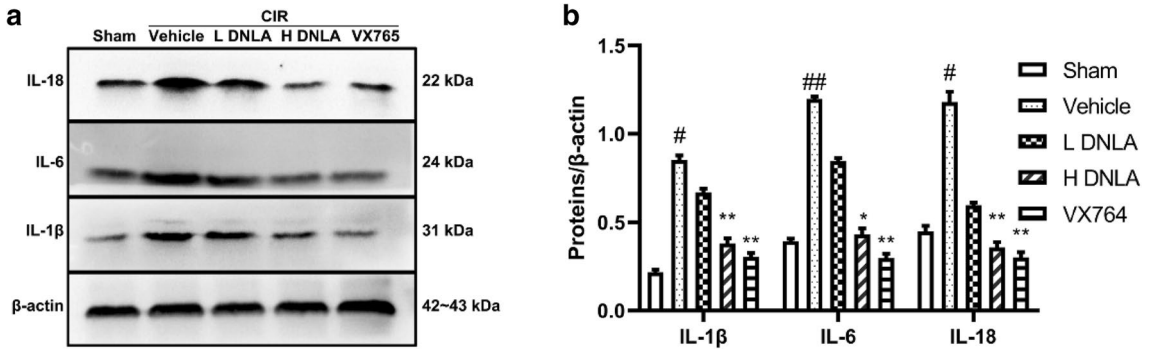

Fig. 5 DNLA further diminishes the activation of IL-1β, IL-6 and IL-18 in the hippocampal CA1 region at 24 h after transient cerebral ischemia in mice. **a** Representative Western blot showing the expression of IL-1β, IL-6 and IL-18 in mouse cerebral CA1 region (n = 6). **b** Quantification of the average levels of IL-1β, Il-6, and IL-18 from Western blot. Error bars depict the SD. All values are expressed as percent change relative to control group and were corrected by the level of β-actin. $^{\#\#}P < 0.01$ versus Sham group; $^{\#}P < 0.05$ versus Sham group; $^{**}P < 0.01$ versus Vehicle group; $^{*}P < 0.05$ versus Vehicle group

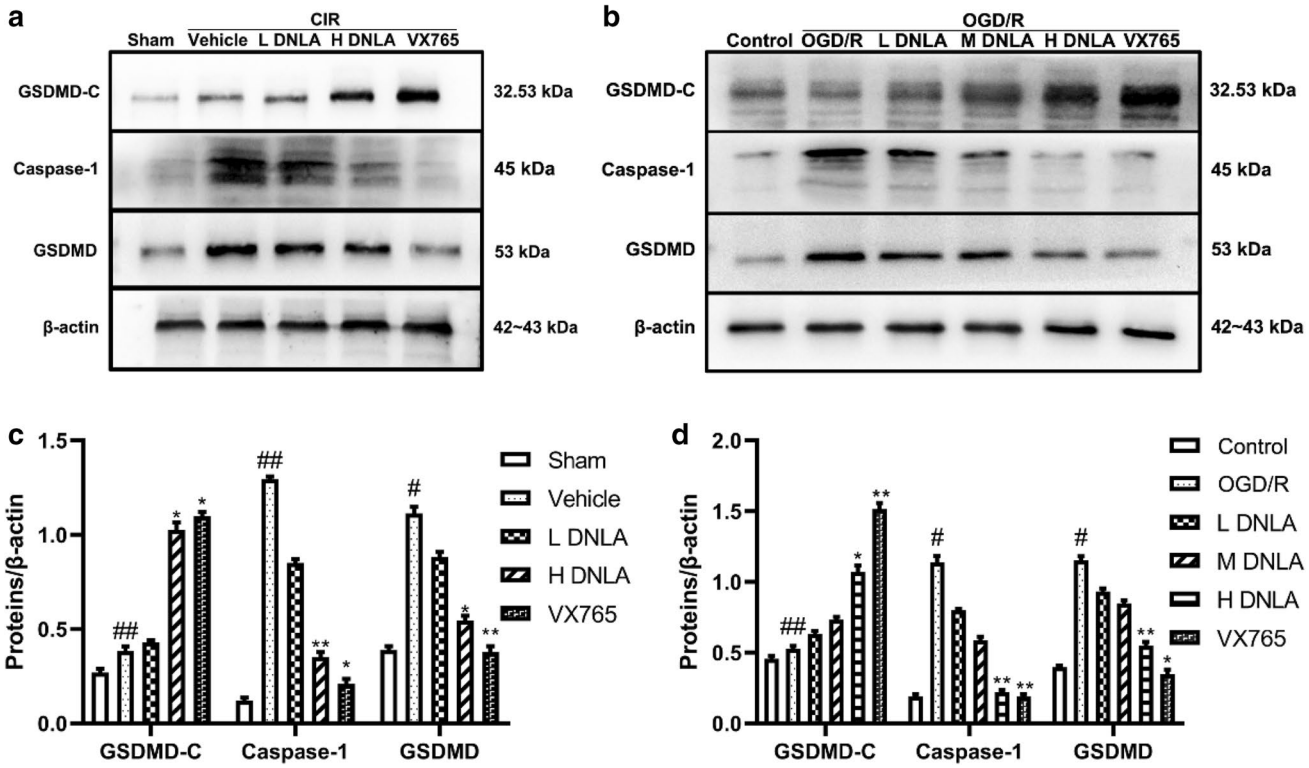

Fig. 6 DNLA prevents pyroptotic death of hippocampal CA1 neurons induced by ischemic injury through inhibition of caspase-1. **a** Western blot analysis of Caspase-1, GSDMD and GSDMD-C after CIR in mouse cerebral CA1 region (n = 6). **b** Western blot analysis of Caspase-1, GSDMD, GSDMD-C at 24 h after oxygen glucose deprivation (OGD) in Ht22 cells (n = 6). **c** Quantification of the expression of Caspase-1, GSDMD, and GSDMD-C in the mouse CA1 region in each group, determined via Western blot. **d** Quantification of the expression of Caspase-1, GSDMD, and GSDMD-C in HT22 cells of each group, determined via Western blot. $^{\#\#}P < 0.01$ versus Sham group; $^{\#}P < 0.05$ versus Sham group; $^{**}P < 0.01$ versus Vehicle group; $^{*}P < 0.05$ versus Vehicle group; $^{\#\#}P < 0.01$ versus Control group; $^{\#}P < 0.05$ versus Control group; $^{**}P < 0.01$ versus OGD/R group; $^{*}P < 0.05$ versus OGD/R group

In our in vitro experiment, we observed that LDH was released weakly from HT22 cells after 24 h of OGD/R cultured with PEG3000, though once PEG3000 was added into routine culture, LDH release increased [40]. Larger PEGs are typically not used because of their proven cytotoxicity. Our data therefore imply the occurrence of pyroptosis in

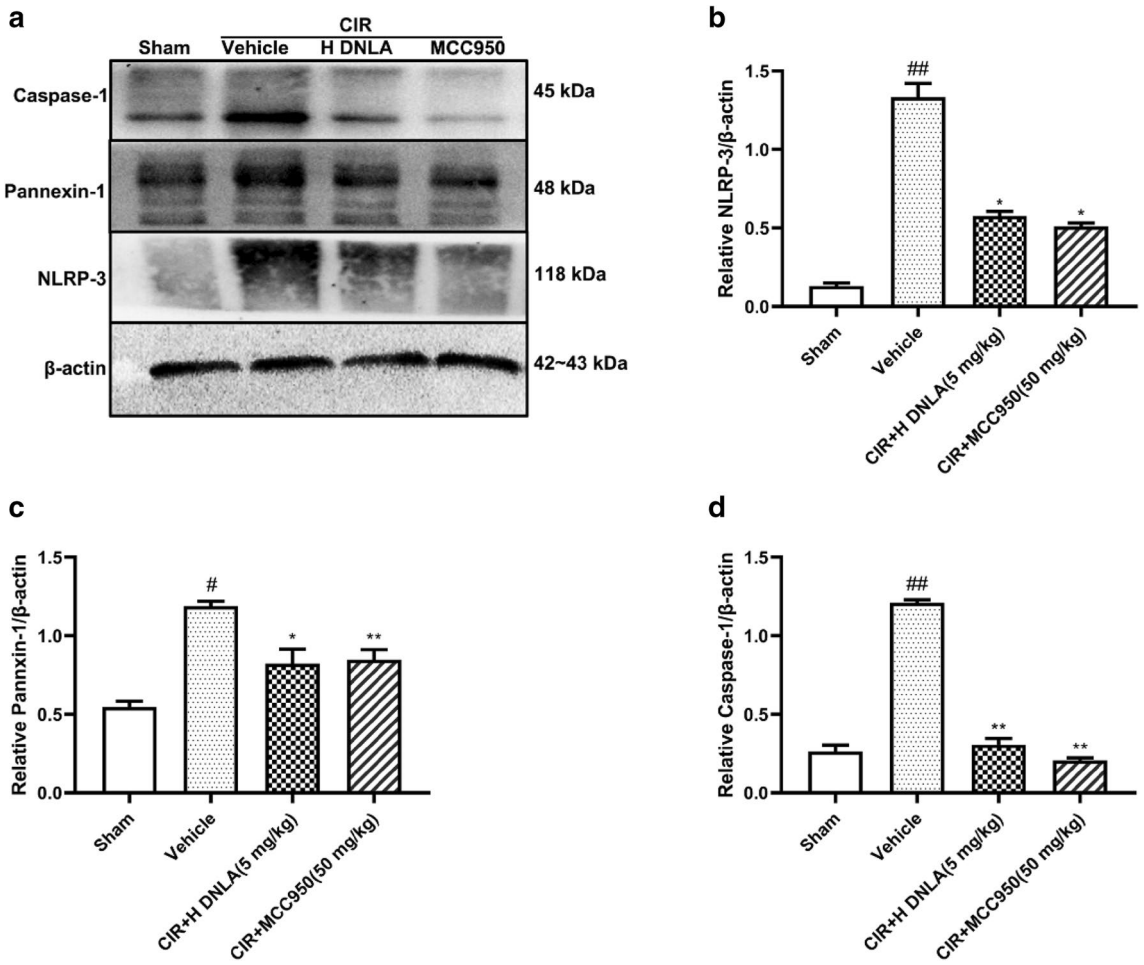

Fig. 7 Effects of DNLA pretreatment on the expression of NLRP-3, Caspase-1, and Pannexin-1 extracted from mouse cerebral hippocampus 24 h after reperfusion. **a** NLRP-3, Caspase-1, and Pannexin-1 expression were assessed by Western blot analysis using the corresponding antibody and the β-actin loading control antibody(n = 6). **b** Quantification results are shown for the NLRP-3 immunoblot data presented; **c** quantification results are shown for the Pannexin-1 immunoblot data presented; d Quantification results are shown for the Caspase-1 immunoblot data presented. $^{\#\#}P < 0.01$ versus Sham group; $^{\#}P < 0.05$ versus Sham group; $^{**}P < 0.01$ versus Vehicle group; $^{*}P < 0.05$ versus Vehicle group

the hippocampal CA1 region and suggest that DNLA exert cerebral neuroprotection by blocking pyroptotic cell death.

Pyroptotic lytic cell death is dependent on the NLR-mediated activation of Caspase-1 [41, 42], which promotes the secretion of IL-1β, IL-6, and IL-18 and induces the expression of GSDMD [14]. NLRP3, a crucial member of the NLR family, can recognize some damage-associated molecular patterns (DAMPs) [43] and pathogen-associated molecular patterns (PAMPs) such as heat shock proteins and S100 proteins that can also activate Toll-like receptors and thus perpetuate the inflammatory cascade reactions [44]. However, the mechanisms underlying ischemic cerebral vascular disease-associated pyroptotic neuronal death have not yet been discovered. Pretreatment with DNLA significantly decreased neurological deficit score and cerebral infarct volume, and maintained the integrity of the neuronal membrane, Nissl bodies, and organelles, proving that DNLA elicit neuroprotective effects against ischemic disease. Simultaneously, after CIR injury, the expression of Caspase-1 was significantly lower in the DNLA groups than the CIR group. Thus, we believe that the Caspase-1-mediated pyroptotic canonical inflammasome pathway, which can be effectively targeted and inhibited by DNLA, serves as the principal mechanism of CIR-induced hippocampal CA1 region impairment, rather than the pyroptotic uncanonical inflammasome pathway which is directly activated by intracellular bacterial lipopolysaccharide [45].

There is mounting evidence indicating that NLRP3 assembles pro-Caspase-1, triggering a signal cascade that is crucial for the production of inflammatory cytokines such as IL-1β, IL-6, and IL-18 in parallel with other well-established signal cascades mounted by TLRs [46, 47]. The activation of

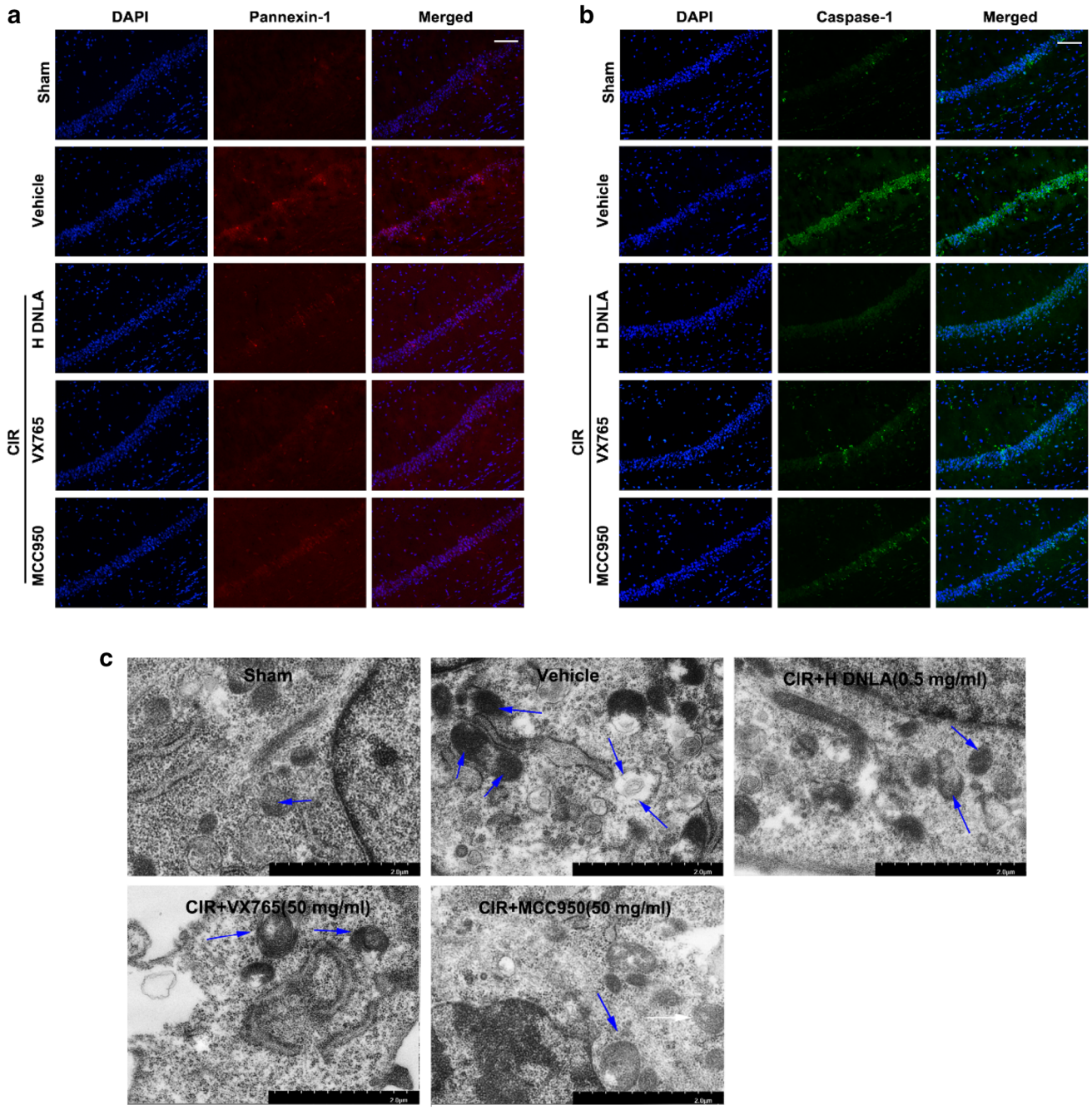

Fig. 8 Inhibition of caspase-1 upon incubation with DNLA attenuates CIR-induced damage in the hippocampal CA1 region in C57/BL mice. **a**, **b** Immunofluorescence staining for Caspase-1 and Pannezin-1 in the hippocampal CA1 region of different groups (n = 3) respectively, Scale bar, 100 μm. **c** Transmission electron microscopy images of neuronal mitochondrial morphological changes in the hippocampal CA1 region of ischemia–reperfusion-challenged C57/BL mice. Blue arrows mark swollen and vacuole-like structures, DNLA inhibit pyroptotic neuronal death via the reactive oxygen species-dependent mitochondrial signaling pathway (n = 3), scale bar, 2 μm

Burton's tyrosine kinase in the infarcted area of the ischemic cerebrum has been shown to be essential for NLRP3 inflammasome activation, Caspase-1 activation, and mature IL-1β production [48]. At present, it is well acknowledged that IL-1β, IL-6, and IL-18 inflict grievous damage to the brain in CIR [49, 50]. These pivotal inflammatory molecules adversely affect neuronal survival and adopt different roles in the progression of stroke damage [51, 52]. IL-1β acts as the promoter of inflammatory reactions, IL-6 serves as the regulator of intercellular adhesion molecule synthesis, and IL-18 functions as a chemotactic cytokine. These molecules coordinate closely and mutually promote each other,

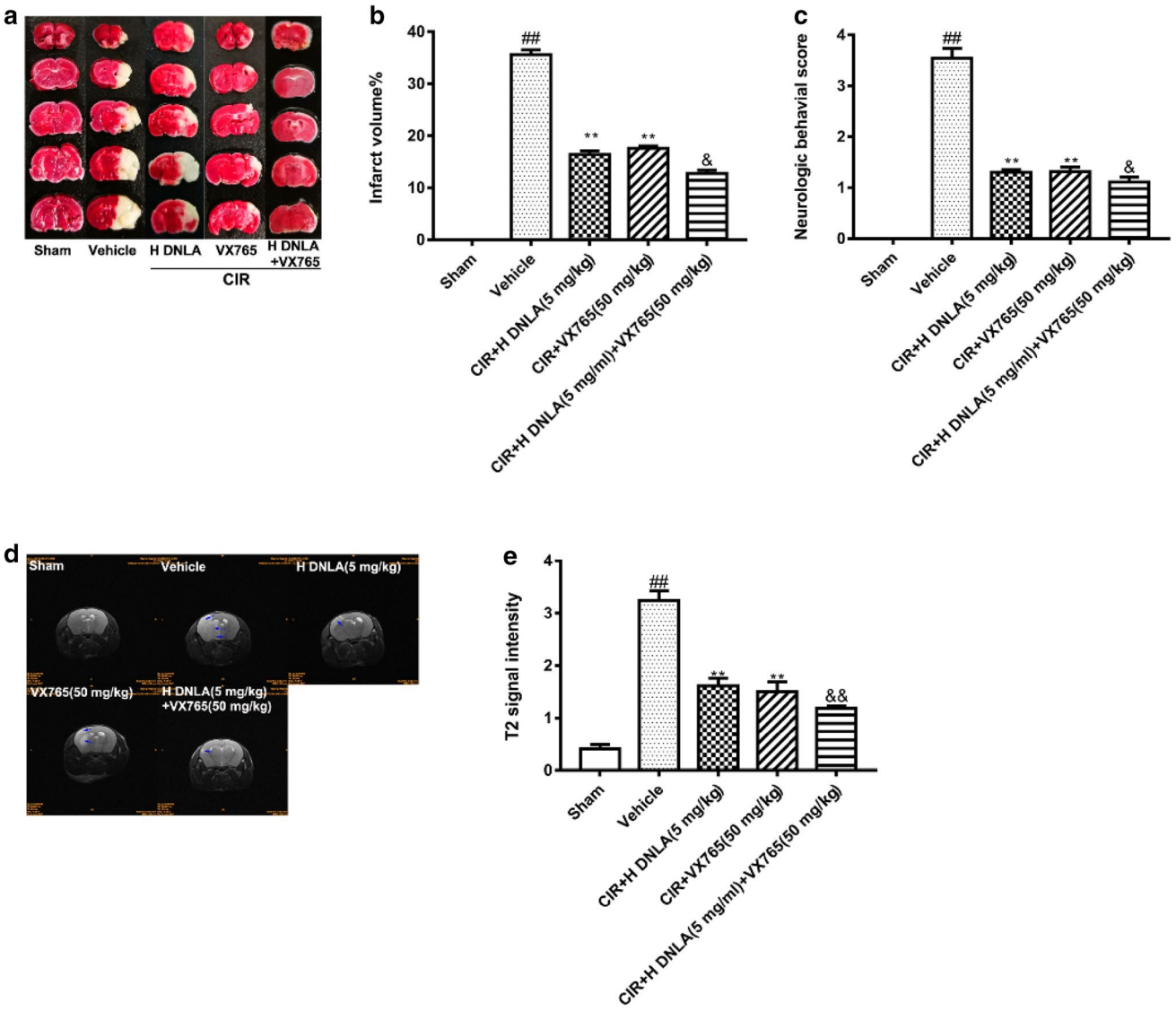

Fig. 9 The Caspase-1 inhibitor VX765 and DNLA exert similar and non-additive neuroprotective effects in mice subjected to CIR injury. **a** Representative images of 2,3,5-Triphenyltetrazolium chloride (TTC)-staining coronal brain sections at 24 h after MCAO (n = 20). **b** Illustration of the cerebral ischemic lesion volume. **c** Illustration of the neurologic deficit score (n = 20). **d** Representative images of T2 weighted signal intensity changes in the ischemia reperfusion region in the mouse brain(n = 6), blue arrows highlight the infarct areas. **e** Quantification of T2 signal intensity in each group. $^{\#\#}P < 0.01$ versus Sham group; $^{**}P < 0.01$ versus Vehicle group; $^{\&\&}P < 0.01$ versus CIR + H DNLA group; $^{\&}P < 0.05$ versus CIR + H DNLA group

inducing an inflammatory cascade and greatly amplifying pyroptotic inflammation [53–55]. We demonstrated that in a mouse model, 24 h of CIR induced increased Caspase-1 protein expression and significantly increased IL-1β, IL-6, and IL-18 expression and activity. However, the expression of IL-1β, IL-6, and IL-18 was significantly reduced in the VX765 and DNLA groups. Our data demonstrate that the binding of DNLA to Caspase-1 could combat CIR-induced cerebral injury by diminishing pyroptosis-induced inflammatory cytokine secretion. Our findings also indirectly verify that IL receptors are abundantly distributed within parts of the hippocampal CA1 region.

Recent studies have shown that GSDMD, a specific substrate of Caspase-1, is a prerequisite effector of the pyroptotic canonical inflammasome pathway [11] and plays an indispensable role in IL-1β secretion but not in IL-1β processing [56]. GSDMD is specifically and precisely cleaved by Caspase-1 into GSDMD-NT and GSDMD-CT. GSDMD-N then typically translocates to the plasma membrane, lysing liposomes and forming pores [57, 58]. GSDMD has been shown to promote the CIR-related NLRP1 and NLRP3, though the mechanism underlying this has not yet been elucidated [11]. A considerable number of GSDMD oligomers recruit NLRP1 and NLRP3, aggravating pyroptotic neuronal

death in the brain. Our in vivo and in vitro findings demonstrated that compared to the CIR group, the expression of GSDMD in the DNLA groups was decreased, particularly in the 3 mg/ml (in vitro) and 5 mg/kg (in vivo) groups. Compared to the CIR group, the expression of GSDMD-C in the DNLA and VX765 groups was increased. These results endorse the previous finding that GSDMD-C autoinhibits GSDMD-N oligomerization [11] in stroke, and demonstrate that DNLA protect against CIR injury via the formation of anti-pyroptotic membrane pores.

Pannexin-1 channels are expressed in the cytoplasm of hippocampal neurons [8], and are thought to serve as ATP release channels [59] and govern inflammasome signaling. Ischemic insults can open Pannexin-1 hemichannels, increasing plasma membrane permeability. This results in imbalances in cellular ions and the loss of cellular energy, together accelerating ischemic neuronal damage [60]. Pannexin-1 further activates the purine receptor P2X7, promoting an amplification loop for the release of intracellular ions and IL-1β [61, 62]. Furthermore, 20 min of ischemia may irreversibly open Pannexin-1 channels irrespective of whether the blood supply to isolated brain neurons is resumed [63]. We unequivocally infer that Pannexin-1 is one of the critical effectors in CIR injury. It has been verified in retinal neurons that Pannexin-1 ablation notably reduces plasma membrane permeation [64]. Our data suggest that Pannexin-1 may mediate NLRP3 inflammasome activation via the same signaling pathway as GSDMD-N, promoting the release of cytokines like IL-1β in central nervous system disease. It is plausible that most Pannexin-1 proteins are present on the surface membrane. Our Western blot and immunofluorescence results both demonstrated a significant increase in Pannexin-1 expression after CIR, and DNLA pretreatment was shown to significantly reduce Pannexin-1 expression. This suggests that the production of ROS, especially nitric oxide, after CIR injury may be involved in Pannexin-1 hemichannel opening [63]. Moreover, in a previous study, co-immunoprecipitation of neuronal lysates indicated that Pannexin-1 closely relates with inflammasome complex components such as Caspase-1 [8], suggesting that Pannexin-1 plays a key role in neuronal pyroptosis in stroke. The opening of Pannexin-1 channels and the formation of membrane pores by GSDMD-N are both involved in the osmotic swelling of neurons, inducing cell lysis and promoting the release of inflammatory factors. All in all, there is a dual directional regulation mechanism between Pannexin-1 and Caspase-1, maintaining membrane integrity and exerting protective effects against CIR injury.

In summary, our results suggest that, in vivo and in vitro, pyroptosis is a form of neuronal death that occurs in the brain after CIR. Additionally, DNLA can ease brain insult in a CIR model via suppressing Caspase-1, thus inhibiting pyroptotic neuronal death and inflammation. Although the occurrence of pyroptosis in other brain regions remains to be investigated, our data suggest the occurrence of pyroptosis in the hippocampal region in stroke. Further research is required to clarify the safety and potential side effects of DNLA, and to explore the more detailed mechanisms of DNLA on CIR impairment.

Materials and Methods

Drugs and Reagents

DNLA (molecular weight: 263.27, CAS: 2115-91-5) was purchased from Chengdu Herbpurify CO., LTD (S-023, Chengdu, China) in 2018 and analyzed by NMR/MS. Alkaloids accounted for 99.87% of DNLA, which mainly contained Dendrobine ($C_{16}H_{25}O_2N$, 98.62%), Nobilonine ($C_{17}H_{27}O_3N$, 0.55%), Dendrobine-N-oxide ($C_{16}H_{25}O_3N$, 0.81%). VX765 (molecular weight: 509, CAS: 273404-37-8, molecular formula: $C_{24}H_{33}ClN_4O_6$) was purchased from Selleck Chemicals (S2228, USA) in 2018. MCC950 (molecular weight: 426.46, CAS: 256373-96-3, molecular formula: $C_{20}H_{23}N_2O_5SNa$) was purchased from Selleck Chemicals (S7809, USA) in 2018.

OGD/R Model

HT22 cells (cell line) were cultured in F12 nutrient medium (Gibco, Carlsbad, CA, USA) supplemented with 5% fetal bovine serum (Gibco) and 0.5% penicillin–streptomycin (penicillin: 100 U/ml, streptomycin: 100 g/ml; Sigma-Aldrich, St. Louis, MO, USA), in a humidified atmosphere at 37 °C under 5% CO_2. To mimic the CIR conditions in vitro, the HT22 cells were cultured under normal conditions for 24 h, then moved to glucose-free DMEM (Gibco) and placed under ischemic conditions (3% O_2, 92% N_2, 5% CO_2) at 37 °C for 2 h. After that, the medium was discarded and the cells were cultured in normal medium under normoxic conditions for another 24 h reperfusion.

Animals

This protocol was approved by the Institutional Animal Care and Use Committee of Chongqing Medical University. Adult male C57BL/6 mice (20–25 g, n = 158) were obtained from the Experimental Animal Center, Chongqing Medical University (Chongqing, China) and kept in individual ventilated cages. All animal studies were approved by the Experimental Ethics Committee of Chongqing Medical University (Reference Number: 22015027), and were performed in accordance with the Chinese Animal Care and Use Guidelines. All surgeries were performed under anesthesia, and all efforts were made to minimize the animals' suffering.

The mice were randomly divided into five groups (n = 25 in each group): the sham-operated group (Sham), the CIR group (Vehicle CIR group), the DNLA-pretreated CIR group (low dose = 0.5 mg/kg, high dose = 5 mg/kg), the MCC950-pretreated CIR group (optimal dose = 50 mg/kg), and the VX765-pretreated CIR group (optimal dose = 50 mg/kg).

Middle Cerebral Artery Occlusion Model

Male mice were fasted for 12 h before surgery. The mice were then anesthetized with pentobarbital sodium (40 mg/kg, ip). The right common carotid artery (CCA), external carotid artery (ECA), and internal carotid artery (ICA) were identified and separated carefully under a stereo dissecting microscope (Belona, Shanghai, China). A 6–0 nylon monofilament (Guangzhou Jialing Biotechnology Co., Ltd., Guangzhou, China) was applied through the stump of the CCA into the ICA and inserted until gentle resistance was felt. The nylon monofilament was removed from the bifurcation after 60 min of occlusion, and reperfusion then lasted for 24 h. The sham-operated mice underwent the same procedure but the nylon monofilament was not inserted. The rectal temperature of the mice was strictly monitored and maintained between 36.5–37.5 °C by placing the mice in the supine position on a heating pad. Two mice that did not exhibit typical ischemia were removed from the study.

Neurological Assessment

Behavior testing is also critical for observing the degree of ischemia after 24 h of reperfusion. Three blinded researchers rated and recorded the neurological deficit of the mice, and the scores of all the groups were then calculated. The 5-level 4-point Longa method was conducted in this study to evaluate the neurological deficit of each mouse [65]. The criteria for scoring were as follows:

Grade 0: No neurological deficits.
Grade 1: The contralateral forelimb cannot be stretched completely when the mouse is lifted by its tail.
Grade 2: The mouse spontaneously circles to the paralytic side when walking.
Grade 3: The mouse involuntarily falls down to the contralateral side when walking.
Grade 4: The mouse cannot walk automatically and loses consciousness.

Evaluation of Infarct Volume

Two, three, five-Triphenyltetrazolium chloride (TTC) stained brain sections were used to assess cerebral infarct volume. Twenty-four h after reperfusion, immediately after sacrifice, the brains were removed from the mice and cut coronally into five serial 2-mm slices. Samples were then incubated for 15 min in 2% TTC (Sigma-Aldrich, Hangzhou, China) at 37 °C and fixed in 4% paraformaldehyde overnight. Infarctions remained unstained by TTC. Each brain section of each mouse was stained with TTC (unstained areas were recognized as infarctions) and was evaluated quantitatively using Image-Pro Plus software to calculate the percentage infarct volume.

Western Blot Assessment

Properly anaesthetized mice (n = 24) were decapitated to obtain the right brain tissues, after which, tissues were rapidly extracted on ice, weighted and grinded in liquid nitrogen, then 18 mg homogenates were weighted approximately. The frozen tissue powder was transferred to a 1.5 ml centrifuge tube with RAPI lysis buffer (P00113D; Beyotime, Shanghai, China) that contained proteinase and phosphatase inhibitor cocktail and centrifuged at 12,000 rpm for 15 min at 4 °C. The protein samples were quantified with a bicinchoninic acid protein assay kit (P0012S, Beyotime, China). The protein was separated using sodium dodecyl sulfate-pol-yacrylamide gel electrophoresis (SDS-PAGE) (P0012A, Beyotime, China) with a 12% polyacrylamide gel, and then transferred to polyvinylidene fluoride (PVDF) membrane. Then the membranes were blocked with 5% BSA and incubated 2 h at room temperature and then incubated with primary antibodies over night at 4 °C with the following primary antibodies: rabbit polyclonal anti-IL-1β (16806-1-AP, Proteintech, Wuhan, China, 1:200), rabbit polyclonal anti-IL-6 (21865-1-AP, Proteintech, Wuhan, China, 1:1000), rabbit polyclonal anti-IL-18 (ab71495, Abcam, Cambridge, UK,1:1000), rabbit polyclonalanti-Caspase-1 (ab1872, Abcam, Cambridge, UK,1:500), rabbit monoclonal anti-GSDMD (ab209845, Abcam, Cambridge, UK,1:1000), rabbit monoclonal anti-NLRP3 (ab210491, Abcam, Cambridge, UK,1:1000), rabbit polyclonal anti-PANX1 (12595-1-AP, Proteintech, Wuhan, China, 1:800), rabbit polyclonal anti-β-actin (20536-1-AP, Proteintech, Wuhan, China,1:1000). After three washes, the membranes were incubated with secondary antibodies HRP-labeled Goat Anti-Rabbit IgG (H + L) (SA00003-2, Proteintech, Wuhan, China, 1:2000) and HRP-labeled Goat Anti-Rat IgG (H + L) (SA00003-11, Proteintech, Wuhan, China, 1:500) for 1 h at room temperature. β-actin was used as loading control. The immune bands were detected with an ECL kit (Advansta, Menlo Park, CA, USA), and analyzed by the ChemiDoc detection system and Quantity One software (Bio-Rad, Hercules, CA, USA).

Magnetic Resonance Imaging

This experiment was conducted using an advanced 1.5 T nuclear magnetic resonance system (Siemens, Germany,

Army Medical University) after 24 h of reperfusion. Mice were anesthetized using isoflurane, a new inhaled anesthetic with quick inspiration, rapid induction, and fine controllability [66]. Cerebral infarction was evaluated and assessed by T2-weighted intensified scanning that precisely imaged the right hippocampus [67]. The size of the infarct was then calculated using MRI software.

Scanning Electron Microscope

Foaming of pyroptotic cells was evaluated by using SEM. Cells were fixed with 4% glutaraldehyde overnight, and then rinsed with PBS three times and dried in the critical point dryer (K850, Quorum). Dried specimens were applied on the conductive carbon film (MSP-2S, IXRF) and sputter coated with gold, and then observed under scanning electron microscopy (SU8010, HITACHI).

Flow Cytometry (FCM)

HT22 cells were washed with PBS (C0221A; Beyotime, Shanghai, China) and then digested with pancreatin (C0203; Beyotime, Shanghai, China), next to centrifuging at 168×*g* for 5 min after OGD/R. The supermatant was discarded to collect the cells that were resuspended in PBS. The cells in the suspension were counted and labeled with Annexin V (AV) and Propidium Iodide (PI) briefly, after which flow cytometry (Guava easyCyte™ 8, Millipore, USA) was employed to quantitatively determine and meticulously analyze the apoptosis cells.

Immunofluorescence Staining

The penumbra region was determined by immunofluorescence staining. The mice (n = 12) were anesthetized and rapidly perfused with 0.9% sodium chloride and fixed with 4% paraformaldehyde via the coronary sinus. The brains were immediately removed and underwent dehydration using phosphate buffered saline containing 30% sucrose for 12 h. Afterwards, a frozen section machine (Cryotome E, Thermo) was used to section the samples and they were then embedded and frozen in OCT-Freeze medium (4583, Sakura). Cryosections were incubated with 10% goat serum for 2 h at room temperature to block non-specific immunoglobulin binding. Following blocking, the sections were incubated with rabbit anti-Caspase-1 (1:200) and anti-Pannxin-1 (1:200) primary antibodies overnight at 4 °C. After rinsing with PBS gently, the sections were incubated with biotinylated goat anti-rabbit antibodies (BA1105; Boster, Wuhan, China, 1:200) for 1 h at 37 °C using a water bath. The nuclei were then stained using 4′,6-diamidino-2-phenylindole (DAPI, C1006, Beyotime). The sections were observed under a fluorescence microscope (Eclipse C1, Nikon, Japan) and images were collected. Each image captured was then evaluated using Image-Pro Plus 6.0 software.

Immunofluorescence Staining of HT22 Cells

HT22 cells were fixed by 4% paraformaldehyde for 10 min at 24 h after OGD/R. Neurons were incubated with anti-Caspase-1 antibodies (1:200) overnight at 4 °C. Then cells were rinsed by PBS three times and incubated with goat anti-rabbit antibodies (BA1105; Boster, Wuhan, China, 1:200) for 1 h at the 37 °C by using water-bath heating. 4,6-diamidino-2-phenylindole (DAPI, C1006, Beyotime, China) was used to stain the nuclei. Immunoreactive proteins were visualized and imaged by a fluorescence microscope (Eclipse C1, Nikon, Japan).

Nissl Staining

Nissl staining was conducted on the fixed frozen sections (30 μm) to assess the ability of neurons to synthesize proteins. The brain sections were de-fatted by overnight immersion in a 1:1 alcohol/chloroform mixture at room temperature. The slices were then rehydrated using a series of alcohol (100 and 95%) and stained with crystal violet for 5 min. The slides were then washed with distilled water and cleared in xylene for three times, 5 min each time. The staining of the hippocampal CA1 region was routinely analyzed by a researcher blinded to the experimental protocol.

HE Staining

Deeply anaesthetized mice were transcardially perfused with PBS followed by 4% paraformaldehyde. The brains were quickly removed by decapitation and carefully post-fixed. Then the samples were paraffinized and sliced to 5 μm-thick sections. The sections were dewaxed in 2 changes of xylene (10 min each) and rehydrated in 2 changes of absolute ethanol (5 min each), then rinsed by running tap water orderly. Haematoxylin Eosin (H&E) staining was performed to observe the histomorphology. Histology assessment was performed by blinded investigator.

Statistical analysis

Statistical analysis was performed by SPSS v20 software. All data are presented as the mean ± SD and each group was conducted with one-way analysis of variance (ANOVA) test followed by the Tukey's test. The $P < 0.05$ reached statistical significance.

Funding This study was supported financially by the China and Chongqing Science and Technology Commission (KJ1600235) and

Chongqing Science and Technology Commission (CSTC2016jcyj A0268, CSTC2016jcyjA0373).

Compliance with Ethical Standards

Conflict of interest: The authors declare that no competing interests exist.

References

1. Jain KK (2000) Neuroprotection in cerebrovascular disease. Expert Opin Invest Drugs 9:695–711
2. Chi MS, Chan LY (2017) Thrombolytic therapy in acute ischemic stroke in patients not fulfilling conventional criteria. Neurologist 22:219–226
3. Jin R, Yang G, Li G (2010) Inflammatory mechanisms in ischemic stroke: role of inflammatory cells. J Leukoc Biol 87:779–789
4. Tobin MK, Bonds JA, Minshall RD, Pelligrino DA, Testai FD, Lazarov O (2014) Neurogenesis and inflammation after ischemic stroke: what is known and where we go from here. J Cereb Blood Flow Metab 34:1573–1584
5. Wang H, Sun L, Su L, Rizo J, Liu L, Wang LF, Wang FS, Wang X (2014) Mixed lineage kinase domain-like protein MLKL causes necrotic membrane disruption upon phosphorylation by RIP3. Mol Cell 54:133–146
6. Chen X, He WT, Hu L, Li J, Fang Y, Wang X, Xu X, Wang Z, Huang K, Han J (2016) Pyroptosis is driven by non-selective gasdermin-D pore and its morphology is different from MLKL channel-mediated necroptosis. Cell Res 26:1007–1020
7. Xi H, Zhang Y, Xu Y, Yang WY, Jiang X, Sha X, Cheng X, Wang J, Qin X, Yu J, Ji Y, Yang X, Wang H (2016) Caspase-1 inflammasome activation mediates homocysteine-induced pyrop-apoptosis in endothelial cells. Circ Res 118:1525–1539
8. Silverman WR, de Rivero Vaccari JP, Locovei S, Qiu F, Carlsson SK, Scemes E, Keane RW, Dahl G (2009) The pannexin 1 channel activates the inflammasome in neurons and astrocytes. J Biol Chem 284:18143–18151
9. Li SJ, Zhang YF, Ma SH, Yi Y, Yu HY, Pei L, Feng D (2018) The role of NLRP3 inflammasome in stroke and central poststroke pain. Medicine (Baltimore) 97:e11861
10. Lamkanfi M, Mueller JL, Vitari AC, Misaghi S, Fedorova A, Deshayes K, Lee WP, Hoffman HM, Dixit VM (2009) Glyburide inhibits the Cryopyrin/Nalp3 inflammasome. J Cell Biol 187:61–70
11. Shi J, Zhao Y, Wang K, Shi X, Wang Y, Huang H, Zhuang Y, Cai T, Wang F, Shao F (2015) Cleavage of GSDMD by inflammatory caspases determines pyroptotic cell death. Nature 526:660–665
12. Kovacs SB, Miao EA (2017) Gasdermins: effectors of pyroptosis. Trends Cell Biol 27:673–684
13. Zhao Y, Shi J, Shao F (2018) Inflammatory caspases: activation and cleavage of gasdermin-D in vitro and during pyroptosis. Methods Mol Biol 1714:131–148
14. He WT, Wan H, Hu L, Chen P, Wang X, Huang Z, Yang ZH, Zhong CQ, Han J (2015) Gasdermin D is an executor of pyroptosis and required for interleukin-1beta secretion. Cell Res 25:1285–1298
15. Ren H, Kong Y, Liu Z, Zang D, Yang X, Wood K, Li M, Liu Q (2018) Selective NLRP3 (pyrin domain-containing protein 3) inflammasome inhibitor reduces brain injury after intracerebral hemorrhage. Stroke 49:184–192
16. Saresella M, La Rosa F, Piancone F, Zoppis M, Marventano I, Calabrese E, Rainone V, Nemni R, Mancuso R, Clerici M (2016) The NLRP3 and NLRP1 inflammasomes are activated in Alzheimer's disease. Mol Neurodegener 11:23
17. Wannamaker W, Davies R, Namchuk M, Pollard J, Ford P, Ku G, Decker C, Charifson P, Weber P, Germann UA, Kuida K, Randle JC (2007) (S)-1-((S)-2-{[1-(4-amino-3-chloro-phenyl)-methanoyl]-amino}-3,3-dimethyl-butanoy l)-pyrrolidine-2-carboxylic acid ((2R,3S)-2-ethoxy-5-oxo-tetrahydro-furan-3-yl)-amide (VX-765), an orally available selective interleukin (IL)-converting enzyme/caspase-1 inhibitor, exhibits potent anti-inflammatory activities by inhibiting the release of IL-1beta and IL-18. J Pharmacol Exp Ther 321:509–516
18. Zheng SQ, Hong XD, Chen TS, Luo PF, Xiao SC (2017) Effects of caspase-1 inhibitor VX765 on cold-restraint stress-induced acute gastric ulcer in mice. Zhonghua Shao Shang Za Zhi 33:688–693
19. Flores J, Noel A, Foveau B, Lynham J, Lecrux C, LeBlanc AC (2018) Caspase-1 inhibition alleviates cognitive impairment and neuropathology in an Alzheimer's disease mouse model. Nat Commun 9:3916
20. Audia JP, Yang XM, Crockett ES, Housley N, Haq EU, O'Donnell K, Cohen MV, Downey JM, Alvarez DF (2018) Caspase-1 inhibition by VX-765 administered at reperfusion in P2Y12 receptor antagonist-treated rats provides long-term reduction in myocardial infarct size and preservation of ventricular function. Basic Res Cardiol 113:32
21. Ismael S, Zhao L, Nasoohi S, Ishrat T (2018) Inhibition of the NLRP3-inflammasome as a potential approach for neuroprotection after stroke. Sci Rep 8:5971
22. Ebrahimi T, Rust M, Kaiser SN, Slowik A, Beyer C, Koczulla AR, Schulz JB, Habib P, Bach JP (2018) alpha1-antitrypsin mitigates NLRP3-inflammasome activation in amyloid beta1-42-stimulated murine astrocytes. J Neuroinflamm 15:282
23. Xing YM, Chen J, Cui JL, Chen XM, Guo SX (2011) Antimicrobial activity and biodiversity of endophytic fungi in *Dendrobium devonianum* and *Dendrobium thyrsiflorum* from Vietnam. Curr Microbiol 62:1218–1224
24. Yu Z, Gong C, Lu B, Yang L, Sheng Y, Ji L, Wang Z (2015) Dendrobium chrysotoxum Lindl. alleviates diabetic retinopathy by preventing retinal inflammation and tight junction protein decrease. J Diabetes Res https://doi.org/10.1155/2015/518317
25. Zhang GN, Zhong LY, Bligh SW, Guo YL, Zhang CF, Zhang M, Wang ZT, Xu LS (2005) Bi-bicyclic and bi-tricyclic compounds from Dendrobium thyrsiflorum. Phytochemistry 66:1113–1120
26. Li LS, Lu YL, Nie J, Xu YY, Zhang W, Yang WJ, Gong QH, Lu YF, Lu Y, Shi JS (2017) Dendrobium nobile Lindl alkaloid, a novel autophagy inducer, protects against axonal degeneration induced by Abeta25-35 in hippocampus neurons in vitro. CNS Neurosci Ther 23:329–340
27. Zhang AL, Yu M, Xu HH, Si JP (2013) Constituents of *Dendrobium devonianum* and their antioxidant activity. Zhongguo Zhong Yao Za Zhi 38:844–847
28. Zhang Q, An R, Tian X, Yang M, Li M, Lou J, Xu L, Dong Z (2017) Beta-caryophyllene pretreatment alleviates focal cerebral ischemia-reperfusion injury by activating PI3K/Akt signaling pathway. Neurochem Res 42:1459–1469
29. Wang Q, Gong Q, Wu Q, Shi J (2010) Neuroprotective effects of Dendrobium alkaloids on rat cortical neurons injured by oxygen-glucose deprivation and reperfusion. Phytomedicine 17:108–115
30. Rayamajhi M, Zhang Y, Miao EA (2013) Detection of pyroptosis by measuring released lactate dehydrogenase activity. Methods Mol Biol 1040:85–90
31. DiPeso L, Ji DX, Vance RE, Price JV (2017) Cell death and cell lysis are separable events during pyroptosis. Cell Death Discov 3:17070
32. Miao EA, Leaf IA, Treuting PM, Mao DP, Dors M, Sarkar A, Warren SE, Wewers MD, Aderem A (2010) Caspase-1-induced

pyroptosis is an innate immune effector mechanism against intracellular bacteria. Nat Immunol 11:1136–1142
33. Yang M, Lv Y, Tian X, Lou J, An R, Zhang Q, Li M, Xu L, Dong Z (2017) neuroprotective effect of beta-caryophyllene on cerebral ischemia-reperfusion injury via regulation of necroptotic neuronal death and inflammation: in vivo and in vitro. Front Neurosci 11:583
34. Chen D, Yu J, Zhang L (2016) Necroptosis: an alternative cell death program defending against cancer. Biochim Biophys Acta 1865:228–236
35. Ichim G, Tait SW (2016) A fate worse than death: apoptosis as an oncogenic process. Nat Rev Cancer 16:539–548
36. Ribeiro SC, Muratori M, De Geyter M, De Geyter C (2017) TUNEL labeling with BrdUTP/anti-BrdUTP greatly underestimates the level of sperm DNA fragmentation in semen evaluation. PLoS ONE 12:e0181802
37. Han J, Zhong CQ, Zhang DW (2011) Programmed necrosis: backup to and competitor with apoptosis in the immune system. Nat Immunol 12:1143–1149
38. Zhang Y, Chen X, Gueydan C, Han J (2018) Plasma membrane changes during programmed cell deaths. Cell Res 28:9–21
39. Russo HM, Rathkey J, Boyd-Tressler A, Katsnelson MA, Abbott DW, Dubyak GR (2016) Active caspase-1 induces plasma membrane pores that precede pyroptotic lysis and are blocked by lanthanides. J Immunol 197:1353–1367
40. Brennan MA, Cookson BT (2000) Salmonella induces macrophage death by caspase-1-dependent necrosis. Mol Microbiol 38:31–40
41. Lamkanfi M, Dixit VM (2014) Mechanisms and functions of inflammasomes. Cell 157:1013–1022
42. Mahla RS, Reddy MC, Prasad DV, Kumar H (2013) Sweeten PAMPs: Role of Sugar Complexed PAMPs in Innate Immunity and Vaccine Biology. Front Immunol 4:248
43. Shichita T, Ito M, Yoshimura A (2014) Post-ischemic inflammation regulates neural damage and protection. Front Cell Neurosci 8:319
44. Rai V, Agrawal DK (2017) The role of damage- and pathogen-associated molecular patterns in inflammation-mediated vulnerability of atherosclerotic plaques. Can J Physiol Pharmacol 95:1245–1253
45. Nossek H, Thierichen A (1989) Dependence of bleeding provocation on the probing force for diagnostics and progress evaluation of inflammatory periodontal diseases. Stomatol DDR 39:530–536
46. Fink SL, Cookson BT (2005) Apoptosis, pyroptosis, and necrosis: mechanistic description of dead and dying eukaryotic cells. Infect Immun 73:1907–1916
47. Kufer TA, Sansonetti PJ (2007) Sensing of bacteria: NOD a lonely job. Curr Opin Microbiol 10:62–69
48. Ito M, Shichita T, Okada M, Komine R, Noguchi Y, Yoshimura A, Morita R (2015) Bruton's tyrosine kinase is essential for NLRP3 inflammasome activation and contributes to ischaemic brain injury. Nat Commun 6:7360
49. Li Y, Xu L, Zeng K, Xu Z, Suo D, Peng L, Ren T, Sun Z, Yang W, Jin X, Yang L (2017) Propane-2-sulfonic acid octadec-9-enyl-amide, a novel PPARalpha/gamma dual agonist, protects against ischemia-induced brain damage in mice by inhibiting inflammatory responses. Brain Behav Immun 66:289–301
50. Zhao GC, Yuan YL, Chai FR, Ji FJ (2017) Effect of Melilotus officinalis extract on the apoptosis of brain tissues by altering cerebral thrombosis and inflammatory mediators in acute cerebral ischemia. Biomed Pharmacother 89:1346–1352
51. Sobowale OA, Parry-Jones AR, Smith CJ, Tyrrell PJ, Rothwell NJ, Allan SM (2016) Interleukin-1 in stroke: from bench to bedside. Stroke 47:2160–2167
52. Wytrykowska A, Prosba-Mackiewicz M, Nyka WM (2016) IL-1beta, TNF-alpha, and IL-6 levels in gingival fluid and serum of patients with ischemic stroke. J Oral Sci 58:509–513
53. Dutta P, Courties G, Wei Y, Leuschner F, Gorbatov R, Robbins CS, Iwamoto Y, Thompson B, Carlson AL, Heidt T, Majmudar MD, Lasitschka F, Etzrodt M, Waterman P, Waring MT, Chicoine AT, van der Laan AM, Niessen HW, Piek JJ, Rubin BB, Butany J, Stone JR, Katus HA, Murphy SA, Morrow DA, Sabatine MS, Vinegoni C, Moskowitz MA, Pittet MJ, Libby P, Lin CP, Swirski FK, Weissleder R, Nahrendorf M (2012) Myocardial infarction accelerates atherosclerosis. Nature 487:325–329
54. Slaats J, Ten Oever J, van de Veerdonk FL, Netea MG (2016) IL-1beta/IL-6/CRP and IL-18/ferritin: distinct inflammatory programs in infections. PLoS Pathog 12:e1005973
55. Toldo S, Mezzaroma E, O'Brien L, Marchetti C, Seropian IM, Voelkel NF, Van Tassell BW, Dinarello CA, Abbate A (2014) Interleukin-18 mediates interleukin-1-induced cardiac dysfunction. Am J Physiol Heart Circ Physiol 306:H1025–H1031
56. Kayagaki N, Stowe IB, Lee BL, O'Rourke K, Anderson K, Warming S, Cuellar T, Haley B, Roose-Girma M, Phung QT, Liu PS, Lill JR, Li H, Wu J, Kummerfeld S, Zhang J, Lee WP, Snipas SJ, Salvesen GS, Morris LX, Fitzgerald L, Zhang Y, Bertram EM, Goodnow CC, Dixit VM (2015) Caspase-11 cleaves gasdermin D for non-canonical inflammasome signalling. Nature 526:666–671
57. Ding J, Wang K, Liu W, She Y, Sun Q, Shi J, Sun H, Wang DC, Shao F (2016) Pore-forming activity and structural autoinhibition of the gasdermin family. Nature 535:111–116
58. Sborgi L, Ruhl S, Mulvihill E, Pipercevic J, Heilig R, Stahlberg H, Farady CJ, Muller DJ, Broz P, Hiller S (2016) GSDMD membrane pore formation constitutes the mechanism of pyroptotic cell death. EMBO J 35:1766–1778
59. Brody H (2003) Bounce of a tennis ball. J Sci Med Sport 6:113–119
60. Thompson RJ, Zhou N, MacVicar BA (2006) Ischemia opens neuronal gap junction hemichannels. Science 312:924–927
61. Braun J, Schultek T, Tegtmeier KF, Florenz A, Rohde C, Wood WG (1986) Luminometric assays of seven acute-phase proteins in minimal volumes of serum, plasma, sputum, and bronchioalveolar lavage. Clin Chem 32:743–747
62. Yang D, He Y, Munoz-Planillo R, Liu Q, Nunez G (2015) Caspase-11 requires the pannexin-1 channel and the purinergic P2X7 pore to mediate pyroptosis and endotoxic shock. Immunity 43:923–932
63. Zhang L, Deng T, Sun Y, Liu K, Yang Y, Zheng X (2008) Role for nitric oxide in permeability of hippocampal neuronal hemichannels during oxygen glucose deprivation. J Neurosci Res 86:2281–2291
64. Dvoriantchikova G, Ivanov D, Barakat D, Grinberg A, Wen R, Slepak VZ, Shestopalov VI (2012) Genetic ablation of Pannexin1 protects retinal neurons from ischemic injury. PLoS ONE 7:e31991
65. Michalski D, Pitsch R, Pillai DR, Mages B, Aleithe S, Grosche J, Martens H, Schlachetzki F, Hartig W (2017) Delayed histochemical alterations within the neurovascular unit due to transient focal cerebral ischemia and experimental treatment with neurotrophic factors. PLoS ONE 12:e0174996
66. Shan J, Sun L, Wang D, Li X (2015) Comparison of the neuroprotective effects and recovery profiles of isoflurane, sevoflurane and desflurane as neurosurgical pre-conditioning on ischemia/reperfusion cerebral injury. Int J Clin Exp Pathol 8:2001–2009
67. Wu D, Zhang J (2016) In vivo mapping of macroscopic neuronal projections in the mouse hippocampus using high-resolution diffusion MRI. Neuroimage 125:84–93